Peer reviewed version

Link to publication record in Explore Bristol Research
PDF-document

University of Bristol - Explore Bristol Research
General rights

In-plane elasticity of a multi re-entrant auxetic honeycomb

E.Harkati[1], N. Daoudi[1], A. Bezazi[2], A. Haddad[2], F. Scarpa[3]

[1]Laboratory of Mines, Tebessa University, route de Constantine, Tébessa-12000, Algeria.   E-mail: harkati.elhaddi@gmail.com

[2] Laboratoire Mécanique appliquée des nouveaux matériaux (LMANM), Département de Génie Mécanique, Faculté des sciences et de la technologie, Université 08 Mai 1945 Guelma 24000 Algérie.

[3]Department of Aerospace Engineering, University of Bristol, BS8 1TR Bristol, UK. E-mail: F.Scarpa@bristol.ac.uk

Abstract: Honeycomb structures are essentially constituted of a repetition of regularly-arranged and loaded sub-structures. The present study carries out a parametrically investigation of the behavior of a multi re-entrant honeycomb structure with variable stiffness and Poisson's ratio effects. A refined analytical model is specifically developed and compared to full-scale numerical simulations. The analytical model developed is based on energy theorems and takes into full consideration bending, shearing and membrane effects. The influence of the cell walls thickness on the elastic homogenized constants is investigated. The results obtained show a good agreement between the refined analytical approach developed and the numerical computations carried out.

Corresponding author: Prof. Abderrezak BEZAZI
Laboratory of Applied Mechanics of New Materials (LMANM), PO Box 401, university 8 Mai 1945, Guelma-24000, Algeria.
 E-mail: ar_bezazi@yahoo.com

Notations:

A : Wall base.

A^* : Shear section decrease.

E_1, E_2 : Young's moduli in directions 1 and 2.

E_s : Young's modulus of basic material.

l : Cell walls lengths.

M : Bending moment.

N : Normal force.

P : Direction 1 concentrated load.

T : Shear force.

t : Cell wall thickness.

U : Elastic strain energy.

u_1, u_2 : Displacement in in directions 1 and 2.

W : Direction 2 concentrated load.

α : Cell aspect ratio, $\left(\alpha = \dfrac{h}{l} \right)$.

β : Wall base aspect ratio, $\left(\beta = \dfrac{a}{l} \right)$.

γ : Wall thickness ratio, $\left(\gamma = \dfrac{t}{l} \right)$.

$\varepsilon_1, \varepsilon_2$: Plane deformation.

θ : Cell internal angle.

v_s : Poisson's ratio of basic material.

φ : Inclination of the base of the wall.

v_{12}, v_{21} : Poisson's ratio in the plane 1-2.

I. Introduction

Cellular materials technology has had a significant development during the past fifty years. Whether they are natural or synthetic, these low density and high specific rigidity materials have seen a widening of their use, in particular during the last twenty years when their production has increased significantly [1][2]. Cellular materials represent an important class of solids that may be used in a variety of engineering applications. Research studies on such systems have been carried out in recent years, particularly about tailored two-dimensional honeycombs [3][4][5][6][7][9]. In most cases, the Poisson's ratio of cellular structures is positive, i.e. the material undergoes a contraction along the direction perpendicular to the one of the load application. However, a negative value of the Poisson's ratio means that the material would laterally expand when stretched, leading to an increase of its volume [8][10][11].

A class of foams that exhibits negative Poisson's ratios has been manufactured and presented for the first time by Lakes [12] back in 1987. The first model of re-entrant structures that shows a negative Poisson's ratio $v = -1$ was introduced back in 1985 by Almgren [13]. The structure was first made in 2D before being extended to 3D. The

model; that may be applied to different geometric structures such as rods, hinges and springs; led to structures that show macroscopic isotropic elastic properties though anisotropic in its microscopic details. Noticing that the molecular dynamics methods with constant pressure or tension displays a fundamental limitation represented by their incapacity to be used to study discontinuous potentials, Wojciechowski [14] applied a constant thermodynamic tension Monte Carlo approach to study the elastic properties of a two-dimensional system of hard cyclic hexamers. His results confirmed the existence of a phase transition between a tilted and a straight phase. He obtained positive results for S12 which corresponds to a negative Poisson's ratio. Furthermore, study the elastic properties of a two-dimensional lattice model has been carried out by the same author on triangular lattice hexagonal molecules [15] and shown to display a negative Poisson's ratio at high densities when the anisotropy of the molecules is substantial. Thought using a completely different analysis, the results of Wojciechowski [4] have been achieved by Rothenburh et al [16] when they interest themselves to a class of microstructures that exhibits a negative Poisson's ratio for large interpenetrations. This behavior is shown to be caused by a greater stiffness of the microstructural elements in shear than in compression. In 1991, Lakes [17] asserted that the Poisson's ratio is governed by aspects of the microstructure identified as the rotational degrees of freedom, the non-affine deformation kinematics or anisotropic structure. Several structures including the chiral microstructure with non-central force interaction or non-affine deformation were examined can also exhibit a negative Poisson's ratio. Geometries that are commonly found in inorganic crystalline materials have been investigated. A model based on microscopic crystal structures was proposed by Ishibashi and Iwata [18], and resulted in a negative Poisson's ratio. A new mechanism that achieves a negative Poisson's ratio has been developed by Grima and Evans [19]. This model has been based on an arrangement comprising rigid squares joined together at their apexes by joints, can be considered as a two-dimensional arrangement or as a projection on a particular plane of a three-dimensional structure. Triangles were also used and joined together in the same way.

Evans et al [20] were the first to term such materials as 'auxetic' (from the word "auxetos" that means 'may be subjected to increase'). The diverse analytical models developed to describe the in-plane and out-of-plane mechanical properties are based essentially on the theory of elastic engineering beams, combined to a series of assumptions related to boundary conditions and specific cell walls mechanisms. When two-dimensionally loaded, the honeycomb-shaped cells may be subjected to bending or stretching of their walls, as well as wall the rotations of the connecting junctions (nodes). Several researchers have developed mathematical models based on these mechanisms. Gibson and Ashby [3] and Gibson et al [21] developed a 2-D model assuming a beam-like bending of the cell walls. Nkansah and Hutchinson [22] however showed that models solely based on bending tend to produce elastic moduli values well over those produced by molecular modeling. In order to improve the bending-based models, Gibson et al [21] and Masters and Evans [23] incorporated the phenomena of stretching and rotation of the cell walls. Lira et al. [24] describes the out-of-plane shear properties of the multi re-entrant honeycomb configurations. The out-of-plane shear represented by G_{13} et G_{23} affects the transverse deformation of a sandwich panel under a given load level the core providing the deformation contribution via out-of-plane shear, and the face skins via plate bending and tension/compression. In 2013, Pozniak et al. [25] simulated two simple models of two-dimensional auxetic foams. In the first model, the ribs forming the cells of the foam were connected at points corresponding to sites of a disordered honeycomb lattice, while in the second, the connections were not point-like but spatial. Triangles centered at the honeycomb lattice points were used for simplicity. Soft, normal and hard joints were considered for each model respectively corresponding to materials with Young's modulus ten times smaller than, equal to and ten times larger than that of the ribs.

Recently, Li et al [26] designed a two-dimensional quadrilateral cellular structure made from bi-material strips. Its thermal deformation behaviors were studied via experimental, analytical and numerical approaches. It has been demonstrated that the temperature influences the cell shape and turn it from convex to concave (or vice

4

versa) leading the Poisson's ratio to move from positive to negative (or vice versa). However, the structure proposed in the present work is made of a sole material, is initially hexagonal in shape, and subjected to mechanical stresses. The proposed new cell is modified to become double reentrant leading the structure.

The present investigation tries to highlight the possibility of increasing the precision of the model through designing the novel honeycomb-shaped cell configurations represented in Figure 1 taking into account the contribution of different stress responses. The analytical model developed is essentially based on the energy theorems along with taking into consideration the shearing and membrane impacts. It is an extension of a previous studies solely based on bending.

2. Theoretical model

An initial analytical model based on bending deformations only of the ribs has been presented in [5]. To take into account the strain energy associated to the shear and normal forces two different loadings are considered in this paper: one along the vertical direction, and the other on the horizontal direction. They are noted 1 and 2 respectively in Figure 2. The analytical model developed is essentially based on the theorem of Castigliano; the honeycomb cell walls are considered as beam elements and simultaneously subjected to the three types of loading - bending, membrane and shear (Fig. 2-a).

The strain energy for the three deformation mechanisms is expressed by:

$$U = U_M + U_N + U_T = \int_0^l \left(\frac{N^2}{2EA} + \frac{M^2}{2EI} + \frac{T^2}{2GA^*} \right) dx \tag{1}$$

According to the Castigliano's theorem, the displacement of a beam under the influence of a force P may be expressed as:

$$u = \frac{\partial U}{\partial P} \tag{2}$$

2.1. Direction 1

For a solid subjected to a linear elastic deformation the energy theorem formulates the strain energy of the three beam elements of the unit cell as a function of the concentrated load P and bending moment M:

$$\left\{ P, M = \frac{P}{2}\left[L \sin(\theta) + 2a \sin(\varphi) \right] \right\} \tag{3}$$

The displacement of the beams system under the concentrated load P can be expressed in the case of bending as:

$$u_1^M = \frac{1}{2}\frac{P}{E_s b}\left(\frac{L}{t}\right)^3 \left[1 - \cos(2\theta) - 8\beta^3 \cos(2\varphi) + 6\beta \cos(2\theta) \right.$$
$$\left. -12\beta^2 \cos(\theta + \varphi) + 12\beta^2 \cos(\theta - \varphi) \right] \tag{4}$$

For the membrane deformation:

$$u_1^N = \frac{1}{2}\frac{P}{E_s b}\left(\frac{L}{t}\right)\left[1 + 2\beta + \cos(2\theta) + 2\beta \cos(2\phi) \right] \tag{5}$$

For the shear deformation, the displacement amounts to:

$$u_1^T = \frac{6(1+\nu_s)}{5}\frac{P}{E_s b}\left(\frac{L}{t}\right)\left[1 + 2\beta - \cos(2\theta) - 2\beta \cos(2\phi) \right] \tag{6}$$

The total displacement for all contributions along the vertical direction is given by:

$$u_1 = u_1^M + u_1^N + u_1^T = \frac{P}{E_s b}\bar{u}_1 = \frac{P}{E_s b}\left\{ \frac{1}{2\gamma^3}\left[1 - \cos(2\theta) - 8\beta^3 \cos(2\phi) + 6\beta + 8\beta^3 - 6\beta \cos(2\theta) \right.\right.$$
$$\left. + 12\beta^2 \cos(\theta - \phi) - 12\beta^2 \cos(\theta + \phi) \right]$$
$$+ \frac{1}{2\gamma}\left[2\beta + 2\beta \cos(2\varphi) + 1 + \cos(2\theta) \right]$$
$$\left. + \frac{6(1+\nu_s)}{5\gamma}\left[2\beta - 2\beta \cos(2\varphi) + 1 - \cos(2\theta) \right] \right\} \tag{7}$$

For a rectangular cross section ($b \times t$) of the cell walls, the stress and corresponding strain along the vertical direction are:

$$\sigma_1 = \frac{P}{b[h + l\sin(\theta) + 2a\sin(\varphi)]} \tag{8}$$

$$\varepsilon_1 = \frac{u_1}{b[l\cos(\theta) + 2a\cos(\varphi)]} \tag{9}$$

The homogenized Young's modulus may be therefore computed as the ratio between the stress (8) and the uniaxial strain (9). After some mathematical manipulations lit is possible to identify the nondimensional homogenized Young's modulus of the honeycomb E_1:

$$\frac{E_1}{E_S} = \frac{\cos(\theta) + 2\beta\sin(\varphi)}{\alpha + \sin(\theta) + 2\beta\sin(\varphi)}\left(\frac{1}{u_1}\right) \tag{10}$$

The classical honeycomb configuration proposed by Gibson & Ashby [3] may be easily retrieved from (10) through imposing φ and β being equal to 0:

$$\frac{E_1}{E_S} = \gamma^3 \frac{\cos(\theta)}{[\alpha + \sin(\theta)]\sin^2(\theta)}\left\{\frac{1}{1 + \gamma^2\left[\cot^2(\theta) + \frac{12}{5}(\nu_S + 1)\right]}\right\} \tag{11}$$

The Poisson's ratio ν_{12} is defined as minus the ratio of the deformations in both directions. Taking $(u_{1\text{-}2})$ as the displacement in the direction 2 generated by that in the direction 1 noted (u_1), the deformation produced by (u_1) in the vertical direction would be:

$$\varepsilon_1 = \frac{u_1}{l\cos(\theta) + 2a\cos(\varphi)} \tag{15}$$

In the horizontal direction, the deformation produced by (u_1) is:

$$\varepsilon_{2\text{-}1} = \frac{u_{2\text{-}1}}{h + l\sin(\theta) + 2a\sin(\varphi)} \tag{16}$$

The horizontal displacement may then be expressed as:

7

$$u_{2-1} = \frac{P}{E_s b} \bar{u}_{2-1} = \frac{P}{E_s b} \left\{ \frac{1}{2\gamma^3} \left[12\beta \cos^2(\theta) - 16\beta^3 \cos^2(\varphi) + 24\beta^2 \cos(\theta)\cos(\varphi) + 1 + \cos(2\theta) \right] \right.$$
$$+ \frac{1}{2\gamma} \left[1 + 2\alpha + 2\beta - 2\beta \cos(2\varphi))\cos(2\theta) \right]$$
$$\left. + \frac{6(1+v_s)}{5\gamma} \left[1 + 2\beta - 2\beta \cos(2\varphi) + \cos(2\theta) \right] \right\} \qquad (17)$$

The Poisson's ratio (v_{12}) is determined as from equations (10, 15 and 17):

$$v_{12} = -\frac{\varepsilon_2}{\varepsilon_1} = -\frac{L\cos(\theta + 2a\cos(\varphi))}{h + L\sin(\theta) + 2a\sin(\varphi)} \left(\frac{\bar{u}_{2-1}}{\bar{u}_1} \right) \qquad (18)$$

If the wall base and the inclination are taken null (i.e. $a=0$ and $\varphi=0$), this leads to the regular cell relationship given by [2]:

$$v_{12} = \frac{\cos^2(\theta)}{[\alpha + \sin(\theta)]\sin(\theta)} \frac{1 - \gamma^2 + \gamma^2 \left(\frac{12}{5} v + \frac{12}{5} \right)}{\left[1 + \gamma^2 \cot^2(\theta) + 2\gamma^2 \left(\frac{6}{5} v + \frac{6}{5} \right) \right]} \qquad (19)$$

2.2. Direction 2

The system including three beam elements constituting the honeycomb cell quarter is simultaneously subjected to three strains represented by bending, membrane and shear (c.f. Fig. 2). The material strain is assumed to be linear and elastic. Applying the stored potential energy theorem and under the following loads:

$$W, M = \frac{W}{2} \left[L\cos(\theta) + 2a\cos(\varphi) \right]$$

The total horizontal displacement for the three strains is represented by the sum of the displacements due to each one, i.e.:

$$u_2 = u_2^M + u_2^N + u_2^T \qquad (20)$$

8

$$u_2 = \frac{P}{E_S b} \bar{u}_2 = \frac{P}{E_S b} \frac{1}{\gamma^3} \left\{ \frac{1}{2} \left[\cos(2\theta) + 16\beta^3 \cos^2(\varphi) + 1 + 12\beta \cos^2(\theta) \right. \right.$$
$$\left. + 24\beta^2 \cos(\theta)\cos(\phi) \right] + \gamma^2 \left[2\beta \sin^2(\phi) \right.$$
$$\left. + \sin^2(\theta + 2\alpha) \right] + \frac{6(1+\nu_S)}{5} \gamma^2 \left[1 + 2\beta \right.$$
$$\left. \left. + \cos(2\theta) + 2\beta \cos(2\phi) \right] \right\}$$

(21)

The Young's modulus (E_2) is computed through following the same procedure presented in (§3.1.1). Consequently, the stress and the corresponding strain in the direction 2 are:

$$\sigma_2 = \frac{W}{b\left[l \cos(\theta) + 2a \cos(\varphi) \right]}$$

(22)

$$\varepsilon_2 = \frac{u_2}{b\left[h + l\sin(\theta) + 2a\sin(\varphi) \right]}$$

(23)

$$\frac{E_2}{E_S} = \frac{\alpha + \sin(\theta) + 2\beta\sin(\varphi)}{\cos(\theta) + 2\beta\cos(\varphi)} \left(\frac{1}{\overline{u}_2} \right)$$

(24)

leading to:

$$\frac{E_2}{E_S} = \frac{\dfrac{\alpha + \sin(\theta) + 2\beta\sin(\phi)}{\cos(\theta) + 2\beta\cos(\phi)}}{\left\{ \dfrac{1}{2\gamma^3} \left[\cos(2\theta) + 16\beta^3 \cos^2(\phi) + 1 + 12\beta \cos^2(\theta) \right. \right.}$$
$$\left. + 24\beta^2 \cos(\theta)\cos(\phi) \right] + \dfrac{1}{2\gamma} \left[1 + 2\beta + 2\alpha \right.$$
$$\left. - \cos(2\theta) - 2\beta\cos(2\phi) \right] + \dfrac{6(1+\nu_s)}{5\gamma} \left[1 + 2\beta \right.$$
$$\left. \left. + \cos(2\theta) + 2\beta\cos(2\phi) \right] \right\}$$

(25)

Again and similarly to what has been performed in the direction 1, the classical honeycomb configuration proposed by Gibson [2] may be easily retrieved through substituting φ and β by 0. This leads to equation (26) expressed below:

$$\frac{E_2}{E_s} = \frac{\left(\dfrac{h}{L} + \sin\theta \right)}{(\cos\theta)^3} \gamma^3 \left(\frac{1}{1 + \gamma^2 \left(\dfrac{2\alpha}{\cos^2\theta} + \tan^2\theta + \dfrac{12}{5}(\nu_s + 1) \right)} \right)$$

(26)

2.2.1. Poisson's coefficient v_{21}

Noted (v_{21}), the Poisson's ratio is expressed as:

$$v_{21} = \frac{\dfrac{\alpha + \sin(\theta) + 2\beta\sin(\phi)}{\cos(\theta) + 2\beta\cos(\phi)}\left\{ \dfrac{\sin(2\theta)}{2} + 3\beta\sin(2\theta) + 6\beta^2\sin(\theta+\phi) + 4\beta^3\sin(2\phi) \right.}{\left\{ \dfrac{1}{2}\left[\cos(2\theta) + 16\beta^3\cos^2(\phi) + 1 + 12\beta\cos^2(\theta) + 24\beta^2\cos(\theta)\cos(\phi)\right] \right.}$$

$$\left. -\gamma^2\left[\dfrac{\sin(2\theta)}{2} + \beta\sin(2\phi)\right] + \dfrac{12\gamma^2(1+v_S)}{5}\left[\dfrac{\sin(2\theta)}{2} + \beta\sin(2\phi)\right] \right\}$$

$$\left. +\gamma^2\left[2\beta\sin^2(\phi) + \sin^2(\theta) + 2\alpha\right] + \dfrac{6\gamma^2(1+v_S)}{5}\left[1 + 2\beta + \cos(2\theta) + 2\beta\cos(2\phi)\right] \right\}$$

(27)

Equation (28) corresponds to that of a regular cell if β and the angle φ are taken equal to 0 and 0° respectively. This results in:

$$v_{21} = \frac{\sin(\theta)[a + \sin(\theta)]}{\cos^2(\theta)} \cdot \frac{1 + \gamma^2\left(\dfrac{7}{5} + \dfrac{12}{5}v_S\right)}{1 + \gamma^2\left[\dfrac{12}{5} + \dfrac{12}{5}v_S + \tan^2(\theta) + \dfrac{2\alpha}{\cos^2(\theta)}\right]}$$

(28)

2.3. In-plane shear modulus G_{12}

The shear modulus in the plane G_{12} is evaluated by introducing the effects of the shear and axial deformations of the vertical and diagonal sides of dimensions $(h/2)$ and (a,l) respectively. The elements' bending is characterized by a rotation of the node that links them, and the linear momentum vanishes at the segment's mid-span section i.e. at $(a,l/2)$ (c.f. Figure 2.b).

The horizontal displacement and the total shear deformations are thus expressed:

$$u_h = \frac{Fh^2}{48E_S I}\left[l + 2a + 2h + \frac{24h}{5}(1+v_S)\left(\frac{t}{l}\right)^2\right]$$

(29)

$$y_h = \frac{Fh^2}{24EI}\left[1 + \frac{2}{l}(a+h)\frac{2}{\dfrac{h}{l}}\left(\frac{12}{5} + \frac{12}{5}v_S\right)\left(\frac{t}{l}\right)^2\right]\frac{1}{\dfrac{h}{l} + \dfrac{2a}{l}\sin(\varphi) + \sin(\theta)}$$

(30)

10

The deformation taking place in the oblique element is also expressed:

$$y_L = \frac{2\left(u_{membrane} + u_{shear}\right)}{L\cos(\theta) + 2a\cos(\varphi)}$$

(31)

$$y_L = \frac{Ft^2}{24EI}\left\langle\left\{1 + [\alpha + \sin(\theta) + 2\beta\sin(\varphi)]\frac{\sin(\theta) + 2\beta\sin(\varphi)}{[\cos(\theta) + 2\beta\cos(\varphi)]^2}\right\}\sin(\theta)\right.$$
$$\left. + \frac{12}{5}(1+\nu_S)\left[\frac{\alpha}{\cos(\theta) + 2\beta\cos(\varphi)}\right]\cos(\theta)\right\rangle$$

(32)

leading to the total strain:

$$\gamma = \gamma_L + \gamma_h = \frac{F}{2E_bt}\left\langle\left\{1 + [\sin(\theta) + 2\beta\sin(\varphi)]\frac{[\alpha + \sin(\theta) + 2\beta\sin(\varphi)]}{[\cos(\theta) + 2\beta\cos(\varphi)]^2}\right\}\sin(\theta)\right.$$
$$+ \left[\frac{1 + 2(\beta + \alpha)}{\gamma^2}\right]\left[\frac{\alpha^2}{\alpha + 2\beta\sin(\varphi) + \sin(\theta)}\right]$$
$$\left. + \frac{12\alpha}{5}(1+\nu_S)\left[\frac{\cos(\theta)}{\cos(\theta) + 2\beta\cos(\varphi)} + \frac{2}{\alpha + 2\beta\sin(\varphi) + \sin(\theta)}\right]\right\rangle$$

(33)

And the shear modulus:

$$G = \frac{\tau}{\gamma} = \frac{G_{12}}{E_S} = \frac{\gamma^3}{S}\left[\frac{\alpha + 2\beta\sin(\varphi) + \sin(\theta)}{\cos(\theta) + 2\beta\cos(\varphi)}\right]$$

(34)

with:

$$S = \alpha^2[1 + 2(\beta + \alpha)] + \gamma^2\left\langle\frac{12\alpha}{5}(1+\nu_S)\left[2 + \frac{\alpha + 2\beta\sin(\varphi) + \sin(\theta)}{\cos(\theta) + 2\beta\cos(\varphi)}\right] + \left\{[\alpha + 2\beta\sin(\varphi)\right.\right.$$
$$\left.\left. + \sin(\theta)] + \frac{[\alpha + 2\beta\sin(\varphi) + \sin(\theta)]^2}{[\cos(\theta) + 2\beta\cos(\varphi)]^2}[\sin(\theta) + 2\beta\sin(\varphi)]\right\}\sin(\theta)\right\rangle$$

In the case of a thin cell where (N) and (T) are neglected:

$$\frac{G_{12}}{E_S} = \frac{\gamma^3}{\alpha^2(1 + 2\beta + 2\alpha)}\left[\frac{\alpha + \sin(\theta) + 2\beta\sin(\varphi)}{\cos(\theta) + 2\beta\cos(\varphi)}\right]$$

(35)

Setting ($a=0$) will get us back to the hexagonal cell modulus when taking into account the axial and shear impacts [2]:

$$G_{12} = E_s \gamma^3 \frac{\alpha + \sin(\theta)}{\alpha^2 \cos(\theta)} \times \frac{1}{(1+2\alpha) + \gamma^2 \left\langle \frac{12}{5\alpha}(1+\nu_s)\{2 + [\alpha + \sin(\theta)]\} \right.}$$
$$\left. + \frac{1}{\alpha^2}[\alpha + \sin(\theta)]\{\sin(\theta) + [\alpha + \sin(\theta)]tg^2(\theta)\} \right\rangle \tag{36}$$

Moreover, and if the axial and shear impacts are neglected, the classical hexagonal cell is found:

$$G_{12} = E_s t^3 \frac{\alpha + \sin(\theta)}{\alpha^2(1+2\alpha)\cos(\theta)} \tag{37}$$

For a regular cell:

$$G_{12} = \frac{1}{\sqrt{3}} E_s \gamma^3 \frac{1}{1 + \left(\frac{33}{10} + \frac{14}{5}\nu_s\right)\gamma^2} \tag{38}$$

3. The Finite Element Model

The main objective of the computational part lies in the computation of the elastic parameters using an implicit finite element numerical approach under Abaqus 6.10 [27] Commercial Code. The model is represented in figure 3. The computation of the various moduli necessitates to imposing a displacement on one side of the representative elementary volume in a given direction, the opposite side being unmoved. Symmetry is taken into account at the boundary conditions, and three simulations are needed to determine the five elastic moduli: the simulation of the tensile stress along the (x, y) direction leads to the determination of Young's moduli E_1 and E_2 along with Poisson's ratios ν_{12} and ν_{21} (figures 3-a and 3-b) while the simulation of the shear stress along the (xy) plane leads to determine the shear moduli G12 (figure 3-c). The periodic boundary conditions impose various bonds a simulation of auxetic foams was discussed by Pozniak et al. [25].

In order to highlight the influence of the cell numbers on the convergence of the results, computations have been undertaken starting by a number of 2 cells to a

12

maximum of 94 cells (figure 3-d). The convergence has been found to be achieved at a number of 49 cells. The authors used a number of 68 cells which is largely sufficient.

Figure 3-e shows the honeycomb-shaped layout structure constituted by cells and representing the elementary volume investigated. Because of its symmetry, the moduli of elasticity (E_1) and (E_2), and the Poisson's ratio (v_{12}) are determined using one quarter of the volume structure. When using the finite element models, two elements have been used. The first is an elastic shell element with reduced integration (S4R). The mesh considered 68 cells and adopted to ensure convergence upon displacements. A second model was prepared using volume elements C3D8R to simulate the in-plane shear modulus versus the different cell geometry parameters (Figure 3-f). For this model 9600 elements were used to ensure convergence. Similarly to the elastic shell element described earlier, symmetry has been taken into account when considering the boundary conditions

By keeping the cell aspect ratio constant (α=1), the longitudinal modulus of elasticity is calculated for different cell internal angles, wall base aspects ratios and thicknesses (i.e. from -25°<θ<+25°, 0.01<β<0.05 and 0.2<γ<0.4). In all cases, the finite element analysis showed that the analytical results correlate well with the numerical ones (figure 4-a for the Poisson's ratio and figure 4-b for the longitudinal modulus of elasticity). In terms of Poisson's ratio, the error is found to be of the order of 5% (figure 4-a) while for the moduli of elasticity, it is again close to 5% (figure 4-b).

The shear modulus of elasticity (G_{12}) is computed for different cell aspect ratios (α and β) and thicknesses (γ=0.004 to 0.15). Also in this case the results show a good correlation between the analytical and finite element models (figure 4-c). The error is always lower than 7%. The various different cell geometry parameters considered for this benchmark are represented in table 1.

Within the range of parameters considered, the Poisson's ratio reaches negative values in the vicinity of θ=-15°. This is essentially due to the strong anisotropy of the medium, as also shown in figure 5 for different cell parameters. This anisotropy is found to be accompanied by a decrease of the Poisson's ratio to a minimum of -5, and this is a,consequence of the bending-membrane-shear strong coupling together with the impact of the stresses along the neighboring walls and its distribution in the re-entrant cell (i.e. for -15° $\leq \theta \leq$ -5°). It is quite worth of notice that, contrary to classical centre-symmetric honeycomb structures, the peak of the anisotropy ratio is not at θ=0°, but shifted by the presence of the base kink (a/l) with the interior angle ϕ different from zero. Large anisotropy is confined in this case to the range of internal negative and small positive cell angles. On the other hand, for internal cell angles greater than 15° ($\theta \geq$ 15°) the domain becomes increasingly isotropic (i.e. $E_1 \cong E_2$). Recall also that the peak of the anisotropy corresponds to a coefficient of Poisson zero.

4. Parametric Results and Discussions

4.1. Effects of the stretching force (*N*), shear force (*T*) and bending moment (*M*)

The displacements, strains and stresses are determined by taking into account both the normal and shear forces along with the bending moment. The main geometry parameter affecting the homogenized engineering constants is the cross-section represented by the wall thickness defined as the non-dimensional ratio ($\gamma=t/l$). The influence of the three parameters (*MNT*) is represented through the variation of the effective modulus of elasticity (E_1) for two values of the wall thickness ratio (tin with γ=0.04, ad thick for γ=0.4), and shown in figure 6.

For the case of a thin wall, a slight difference is noticed between the various mechanisms of deformation with relatively low values for the angles exceeding 10°, and a maximum in the vicinity of θ= 0°. For the thick wall case and for relatively small angles, the impact of the bending moment (*M*) is found to be seven times stronger than those of the forces (c.f. figure 6-b).

14

Because of their low contribution, the influence of the shear and axial strains dues to (N) and (T) are generally neglected [5][21]. The results obtained show that their effect becomes significant only when the thickness parameter exceeds 0.2 (i.e. $\gamma=t/l > 0.2$), the remaining non-dimensional parameters remaining constants (i.e. $\alpha=1$, $\beta=0.2$ and $\varphi=45^{\circ}$).

The variation of the Poisson's ratio with the cell internal angle is represented in Figure 7. Two different behaviors of the cell are noticed. The conventional one (convex, $\theta > 0$) provides positive values of the Poisson's ratio. High values of this parameter ($v_{12}>4$) are obtained in the vicinity of $\theta=0^{\circ}$ for a cell with thin walls (i.e. $\gamma=0.01$) with the sole contribution coming from the bending moment (M). The Poisson's ratio then decreases significantly under the influence of the normal and shear forces N and T. The relative thickness ($\gamma=t/l$) seems to control the coefficient of Poisson (v_{12}); when it increases, this latter decreases accordingly (cf. Figure 8-c). Finally and for the different wall thicknesses (t), the impact of N and T on the modulus of elasticity along the 2-direction (E_2, cf. equation 25) is found to be relatively insignificant compared to the one of the bending moment.

The effect of the shear and axial deformation is generally neglected because of their low contribution in evaluating the cell plane shear modulus. Refined modeling shows that their impact becomes significant for thick cells. As a consequence, it may be stated that the behavior of high specific density honeycombs cannot be described by a wall solely subjected to bending as proposed by earlier investigations introduced above. Indeed, for relative thickness values greater than 0.1 and when taking into account side effects generated by the axial and shear strains, a significant underestimation of the assessment of the in-plane shear modulus G_{12} may be obtained. Finally, it is observed that the hexagonal cells exhibit a much higher resistance to shear than the other configurations investigated.

The impact of the geometrical parameters on the mechanical behavior of the proposed new honeycomb-shaped cell is fundamental. The effect of the relative thickness is represented in Figure 8. The variation of the relative modulus of elasticity (E_1/E_S) as a function of the cell internal angle (θ) for different values of the wall thickness ratio ($\gamma = t/l$) is represented in figure 8-a. The non-dimensional geometric parameters α, β and φ are kept constant and equal to 1; 0.2 and 45° respectively. For a wall thickness ratio (γ) value of 0.4, the modulus of elasticity (E_1) is found to be 5000 times greater than at $\gamma = 0.01$ and 2.5 times greater than at $\gamma = 0.2$. This indicates that $\gamma = 0.4$ is the boundary-value separating a thin wall from a thick one. Maxima are situated in the vicinity of the cell angle value of $\theta = 0^o$ off-centered by the wall base aspect ratio ($\beta = a/l$).

Keeping the non-dimensional geometric parameters constant ($\alpha = 1$, $\beta = 0.2$ and $\varphi = 45^o$), the variation of the elastic modulus (E_2) with the wall thickness ratio (γ) is found to be quasi parabolic (cf. figure 5-b) particularly for cell internal angles $\theta > 0$. The elastic modulus (E_2) reaches a maximum at $\theta = 30^o$ for $\gamma = 0.4$ that corresponds to a thick cell wall, and corresponds to a conventional cell configuration [3].

Auxetic behavior is observed for negative angles, for which the Poisson's ratio exceeds (-5) in thin reentrant cell walls. A negative value of ($\nu_{12} = -6$) for a thin wall ($\gamma = 0.01$) and positive internal cell angles is unusual in structural honeycomb applications. This is due, in this case, to both the geometry of the cell and the arrangement of the walls that produces a positive and perpendicular reaction when submitted to a positive traction. Poisson's ratio is found to become null at $\theta = -5^o$; this could be considered as the symmetry position representing the intersection of all the curves (taking into account the small shift due to the aspect ratio $\beta = 0.2$ and the inclination angle φ).

The variation of Poisson's ratio with the wall thickness and internal cell angles (positive) is represented in figure 9. It is shown to increase, while the thickness decreases.

In figure 9, the differences in the Poisson's ratio values are essentially due to the wall base parameter. The Poisson's ratio v_{12} is found to be proportional to the wall base dimension whatever the deformation mechanisms; the auxetic behavior is actually reduced when β increases, even for the case of negative internal cell angles.

Figure 10 presents the variation of the normalized Young's modulus in both directions (E_1/E_S and E_2/E_S) with the cell internal angle (θ) for different values of the wall base aspect ratio (β) ranging from 0 to 0.4 and for $\gamma=0.3$ and $\alpha=1$. The normalized elasticity modulus along the 1-direction increases for increasing β values (c.f. figure 10-a). It reaches its optimum between $\theta=-13^{\circ}$ and $\theta=-3^{\circ}$ for all the wall base aspect ratio values considered; that indicates the effect of the wall base on the stiffness of the cell under the membrane and shear loads. In the case of a null wall base aspect ratio parameter ($\beta=0$), the elastic modulus (E_1/E_S) match those of a classical hexagonal cell (Equation 14).

Figure 10-b shows the modulus of elasticity along the 2-direction (E_2), which increases for increasing cell angles, in particular for positive ones. The curve representing the variation of (E_2/E_S) for a wall base aspect ratio $\beta=0.4$ indicates that this nondimensional Young's modulus is approximatively eight times smaller than the one for $\beta=0$ (hexagonal cell). Minima of (E_2) values are in the negative cell angles part (i.e., auxetic configurations).

Figure 11-a shows that the shear modulus (G_{12}) significantly decreases with the cell base 'a'. It is almost 1.8 times lower when $a=0.3l$, leading the cell to be less resistant to shear. The variation of (G_{12}) with the wall thickness is found to be quasi-parabolic (figure 10-a). In comparison to conventional cell configurations and negative cell angles the shear modulus decreases by 20 and 8 times for relative densities of 0.01 and 0.6 respectively, and by 8 times for a relative density of 0.6. This is an aspect to consider as a disadvantage for structural applications for which a high shear modulus

in the plane is expected. It is however a feature potentially to exploit for compliance-driven applications, like in the case of morphing skins with high shear deformability [28][28].

Figure 12 presents the cell angle dependence of the in-plane Poisson's ratio (ν_{12}) for different inclination angles of the wall base (φ) starting from 0° and up to 60°. It is found that the structure with $\varphi=0$ leads to the minimum value of ν_{12} corresponding to approximatively -6 at θ equal to -10. This dependence of the Poisson's ratio on direction and the compliance tensor components for the most general case corresponding to the lowest symmetry crystalline structure along with the angular dependence of Poisson's ratio and its mean value for hard disc (HD) system with hard cycle hexamers (HCH) layers have been investigated by Bilski and Wojciechowski [29] in a recent paper.

5. Conclusions

A multi-reentrant cellular honeycomb shaped cell is investigated with extended analytical models considering the different sets of deformation mechanisms occurring in the walls, along with numerical computations. The honeycomb structure topology is based on four main geometry parameters that may be in case optimized. Conventional modeling approaches for honeycomb structures neglect the axial and shear deformations because of their weak contribution in the evaluation of the in-plane stiffness for classical centre-symmetric topologies. The present study shows instead that the impact of both the axial and shear deformations becomes significant for the thick-walled cells as well as those possessing complex geometries. The auxetic effect is essentially due to the geometrical arrangements of the reentrant cell walls, as well as the bending-membrane-shear strong coupling along the walls bases. This leads to a negative plane Poisson's ratio of the order of (-3), and this is particularly interesting for structures where an auxetic behavior is recommended. Quite importantly, one can

tune the Poisson's ratio behavior in the design space and obtain, for example, positive Poisson's ratio effects even in configurations that would have a baseline auxetic performance.

References

[1]. M. Laroussi, *Modeling the behavior of solid foams porosity: a micro-mechanical approach*, Ph.D., ENPC, Champs-sur-Marne, 2002.

[2]. T. Bitzer, *Honeycomb Technology*. Chapman & Hall, London, 1997.

[3]. L. J. Gibson, M. F. Ashby, *Cellular solids structure and properties*, 2nd Ed., Cambridge University press, UK, 1997.

[4]. M. J. Silva, W. C. Hayes and L. J. Gibson, The effects of non-periodic microstructure on the elastic properties of two-dimensional cellular solids, *Int. J. Mech. Sci. 11 (1995) 61–77.*

[5]. Bezazi, F. Scarpa and C. A. Remillat, Novel centre symmetric honeycomb composite structure, *Compos. Struct. 71 (3–4) (2005) 356–64.*

[6]. J N. Grima, R Cauchi, R Gatt, D Attard. Honeycomb composites with auxetic out-of-plane characteristics. *Compos. Struct. 106 (2013), 150-159*

[7]. C Körner, Y Liebold-Ribeiro. A systematic approach to identify cellular auxetic materials. *Smart Mater. Struct. 24 (2015), 025013.*

[8]. J.P.M. Whitty, A. Alderson, P. Myler, B. Kandola. Towards the design of sandwich panel composites with enhanced mechanical and thermal properties by variation of the in-plane Poisson's ratios. *Compos. Part A 34 (2003), 525-534*

[9]. Y Sun, N M. Pugno. In plane stiffness of multifunctional hierarchical honeycombs with negative Poisson's ratio sub-structures. Compos. Struct. 106 (2013), 681-689.

[10]. AA Pozniak, H Kaminski Kedziora, P Kedziora, B Maruszewski, T Strek, T, KW Wojciechowski. Anomalous deformation of auxetic constrained square. *Reviews on Advanced Materials Science, 23(2) (2010), 169-174.*

[11]. T C Lim. *Auxetic Materials and Structures*. Springer, Singapore, 2015.

[12]. R. S. Lakes, Foam Structures with a NegativePoisson's Ratio, Science 235 (1987) 1038–1040.

[13]. R. F. Almgren, An isotropicthree-dimensional structure withPoisson's ratio = -1, Journal of Elasticity 15 (1985) 427–430.

[14]. K.W. Wojciechowski. Constant thermodynamic tension monte carlostudies of elasticproperties of a two-dimensional system of hard cyclichexamers. MolecularPhysics, 61(5):1247–1258, 1987.

[15]. KWWojciechowski. Two-dimensionalisotropic system with a negative poisson ratio. Physics Letters A, 137(1-2):60–64, 1989.

[16]. Rothenburg, L., Berlin, A. A. & Bathurst, R. J. Microstructure of isotropicmaterialswithnegativePoisson's ratio. *Nature* **354**, 470–472 (1991).

[17]. R. S. Lakes, Deformationmechanisms in negativePoisson's ratio materials: structural aspects, Journal of Materials Science 26 (1991) 2287–2292.

[18]. Y. Ishibashi, M. Iwata, A microscopic model of a negativePoisson's ratio in somecrystals, Journal of the Physical Society of Japan 69 (2000) 2702–2703.

[19]. N. Grima, K.E. Evans, Auxeticbehaviorfromrotating squares, Journal of Materials Science Letters 19 (2000) 1563–1565.

[20]. K. E. Evans, M. A. Nkansa, I. J. Hutchinson and S. C. Rogers, Molecular network design *Nature* 353 *(1991) 124.*

[21]. L. J. Gibson, M. F. Ashby, J. Zhang and T. C. Triantafillou, Failure surfaces for cellular materials under multiaxial loads- I. Modelling*, Int. J. Mech. Sci.,* 31 *(9) (1989) 635-663.*

[22]. M. E. Nkansah, K. E. Evans and I. J. Hutchinson, Modelling the mechanical properties of an auxetic-molecular network, Model*. Simul. Mater. SCI. Engin.* 2 (*1994) 337.*

[23]. Masters and Evans, Models for the elastic deformation of honeycombs. Composite. *Strut*. 35 *(1996) 403-422.*

[24]. C. Lira, P. Innocenti, F. Scarpa, Transverse elastic shear of auxetic multi re-entrant honeycombs, *Composite Structures* 90 (2009) 314–322.

[25]. A. A. Pozniak, J Smardzewski and K W Wojciechowski. Computer simulations of auxetic foams in two dimensions. Smart Mater. Struct. 22 (2013) 084009.

[26]. Li, D. Ma, J., Dong, L., and Lakes, R. S., "A bi material structure with Poisson's ratio tunable from positive to negative via temperature control" *Materials Letters*, 181, 285-288 15 October (2016).

[27]. ABAQUS, version CEA 6.10-1 reference manuals, Dassault Systems, Providence, R.I: Abaqus inc., 2010.

[28]. L Asheghian, G Reich, A Enke J Kudva, Shear Morphing Skins − Simulation and Testing of Optimized Design, Journal of Intelligent Materials Systems and Structures, Vol. 22, (2011), 945-960.

[29]. M. Bilski, K. W. Wojciechowski, Physica Status Solidi B-Baic Solid State Physics 253, pp. 1318-1323 (2016).
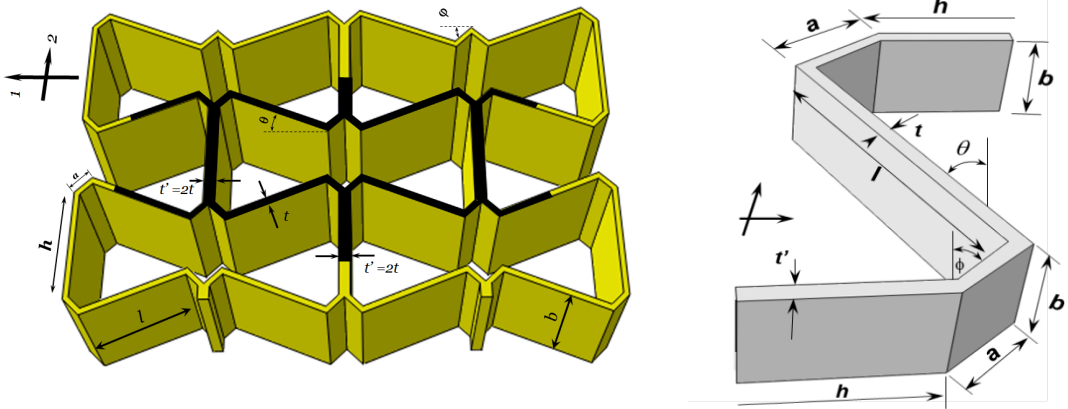
Figure captions

Figure 1. Geometry of the new honeycomb cell: (a) Design of the re-entrant auxetic topology and (b) geometry parameters defining the unit cell

Figure 2. Honeycomb cell models and loads used in the development of the refined model: (a) Global stress distribution for the evaluation of E_1, E_2 and v_{12}; (b) Force distribution to evaluate G_{12}.

Figure 3. Numerical model description. (a) and (b) Boundary conditions taken in the simulation of the tensile along direction 1and 2 respectively. (c) Boundary condition taken in order to determine G_{12}. (d) Dependence of the Poisson's ratio v_{12} and relative modulus E_1/E_s on the computations number of cells. (e): Displacement distribution for a tensile simulation leading to the computation of E_1, E_2 and v_{12}. (f): Model of half a cell and the volume elements used for the computation of G_{12}.

Figure 4. Poisson's ratio, elasticity and shear moduli distribution for $\beta=\gamma=0.2$ and $\varphi=45°$: (a) Poisson's ratio (v_{12}) vs cell angle (θ); (b) Modulus of elasticity in direction 1 (E_1/E_S) vs cell angle (θ); (c) Shear modulus of elasticity (G_{12}/E_S) vs cell angle (θ).

Figure 5. Impact of the effect of the E_1 / E_2 ratio on the variation of the Poisson's coefficient v_{12}. $\beta=\gamma=0.3$ and $\varphi=30°$.

Figure 6. Impact of (MNT) on the effective modulus of elasticity (E_1) for $\alpha=1$, $\beta=0.2$ and $\varphi=45°$(a): $\gamma=t/l=0.04$ and (b): $\gamma=t/l=0.4$

Figure 7. Poisson's ratio and relative modulus of elasticity vs cell internal angle: (a) Influence of the cell internal angle on Poisson's ratio for $\alpha=1$, $\beta=0.2$ and $\varphi=45°$;(b) Influence of the cell internal angle on the relative shear modulus (G_{12}/E_S) for diverse cell configurations and deformation mechanisms ($\alpha=1$, $\beta=0.2$ and $\varphi=45°$).

Figure 8. Effect of the wall thickness: (a) Non-dimensional Young's modulus (E_1/E_S) vs wall thickness ratio ($\gamma=t/l$) for $\alpha=1$, $\beta=0.2$ and $\varphi=45°$; (b) Non-dimensional Young's modulus (E_1/E_S) vs internal cell angle (θ) and wall thickness ratio ($\gamma=t/l$) for $\alpha=1$, $\beta=0.2$ and $\varphi=45°$.

Figure 9. Poisson's ratio (v_{12}) vs internal cell angle (θ) and wall base aspect ratio ($\beta=a/l$).

Figure 10. Effect of the wall base 'a' ($\beta= a/l$): (a) Non-dimensional Young's modulus (E_1/E_S) vs wall base aspect ratio ($\beta= a /l$) for $\alpha=1$, $\gamma=0.3$ and $\varphi=45°$; (b) Non-dimensional Young's modulus (E_2/E_S) vs wall base aspect ratio ($\beta= a /l$) for $\alpha=1$, $\gamma=0.3$ and $\varphi=45°$.

Figure 11. Effect of the wall base 'a' ($\beta= a/l$) Non-dimensional shear modulus (G_{12}/E_S) vs internal cell angle for different wall base aspect ratios ($\beta= a /l$) for $\alpha=1$, $\gamma=0.2$ and $\varphi=20°$.

Figure 12. Cell angle dependence of the in-plane Poisson's ratio.

Figure 1 – Geometry of the new honeycomb cell. (a) Design of the re-entrant auxetic topology and (b) geometry parameters defining the unit cell
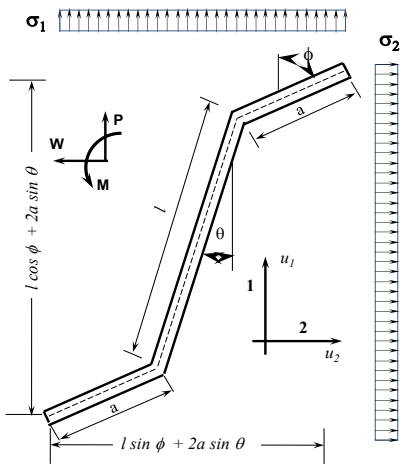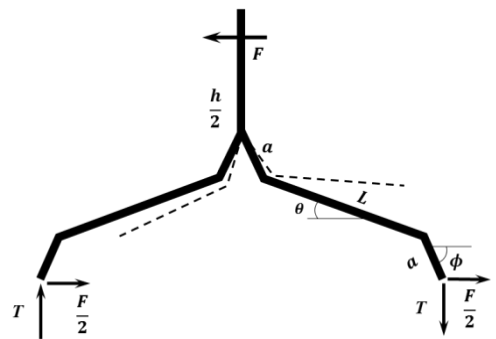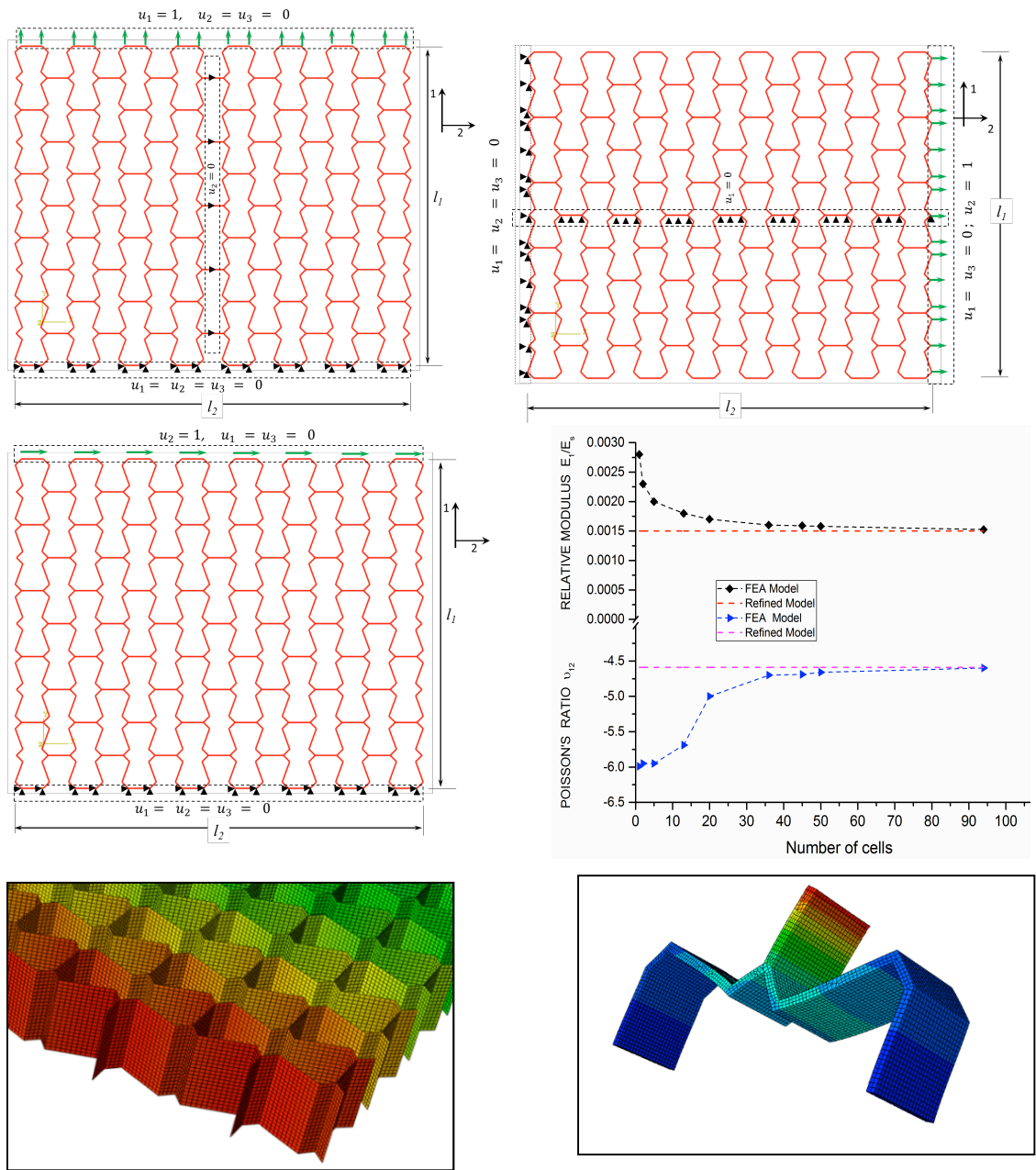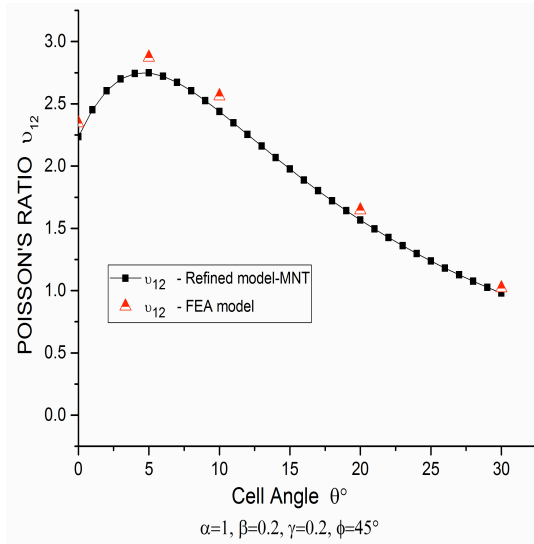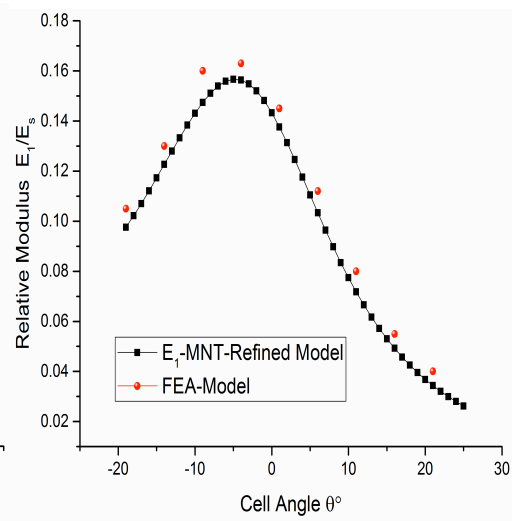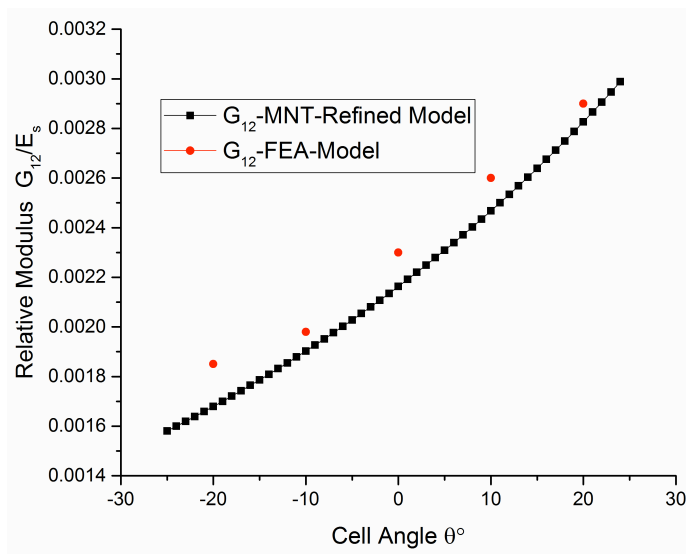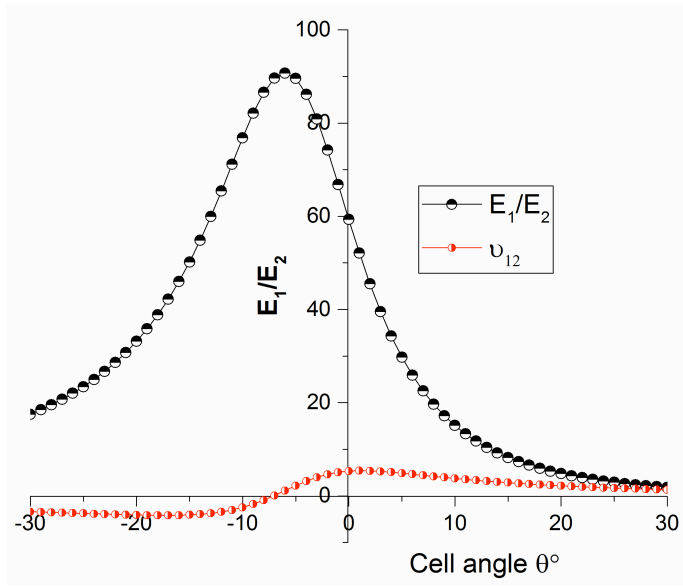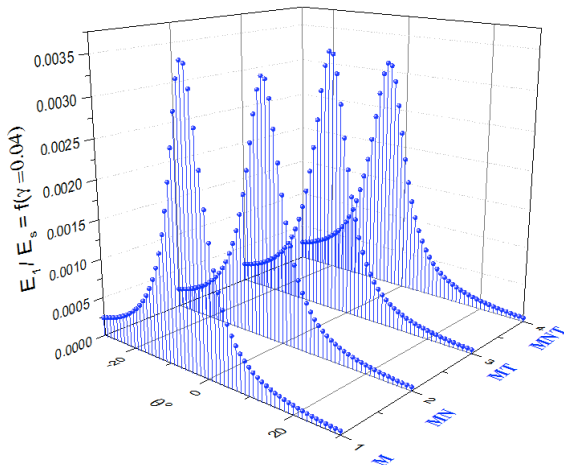

Figure 2-a

Figure 2b

Figure 2: Honeycomb cell models and loads used in the development of the refined model.

(a): Global stress distribution for the evaluation of E_1, E_2 and v_{12}.
(b): Force distribution to evaluate G_{12}.

Figure 3 – Numerical model description.

(a) and (b) Boundary conditions taken in the simulation of the tensile along direction 1and 2 respectively

(c) Boundary condition taken in order to determine G_{12}

(d) Dependence of the Poisson's ratio v_{12} and relative modulus E_1/E_s on the computations number of cells.

(e): Displacement distribution for a tensile simulation leading to the computation of E_1, E_2 and v_{12}.

(f): Model of half a cell and the volume elements used for the computation of G_{12}.

Figure 4-a

Figure 4-b

Figure 4-c

Figure 4 – Poisson's ratio, elasticity and shear moduli distribution for $\beta=\gamma=0.2$ and $\varphi=45°$.
(a): Poisson's ratio (ν_{12}) and (ν_{21}) vs cell angle (θ).
(b): Modulus of elasticity in direction 1 (E_1/E_S) vs cell angle (θ).
(c): Shear modulus of elasticity (G_{12}/E_S) vs cell angle (θ).

Fig.5 Impact of the effect of the E_1 / E_2 ratio on the variation of the Poisson's coefficient v_{12}. $\beta=\gamma=0.3$ and $\varphi=30°$.

Figure 6-a
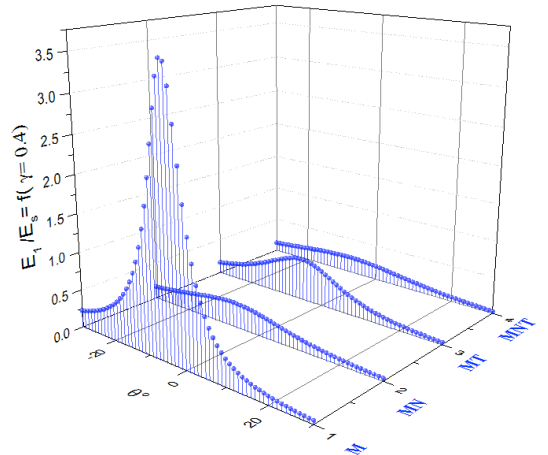
Figure 6-b

Figure 6 – Impact of (*MNT*) on the effective modulus of elasticity (E_1) for $\alpha=1$, $\beta=0.2$ and $\varphi=45°$
(a): $\gamma=t/l=0.04$ and   (b): $\gamma=t/l=0.4$

a)

b)
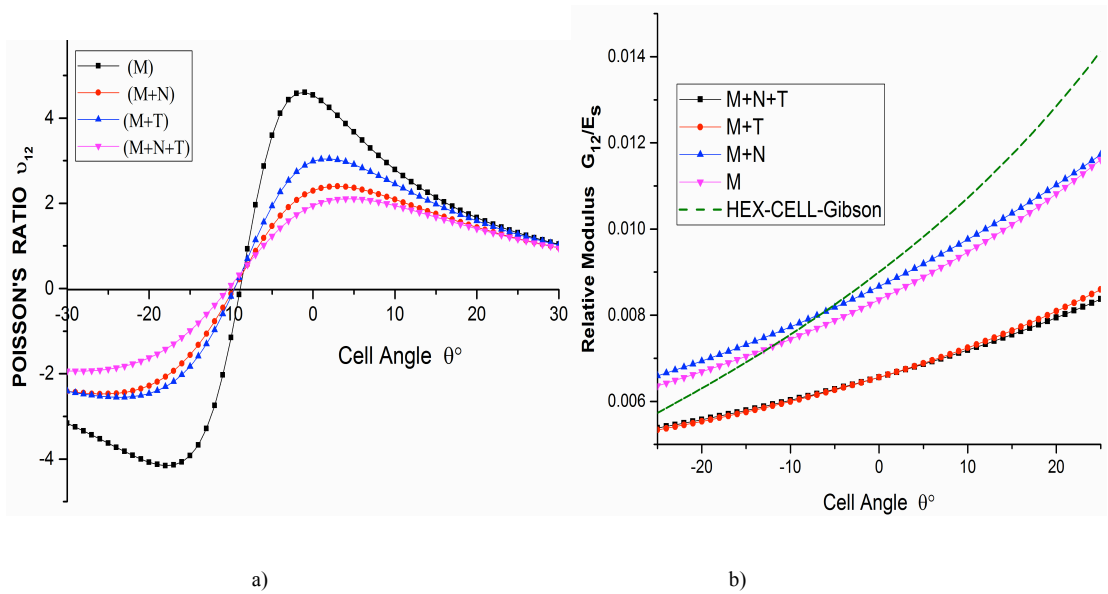
Figure 7 – Poisson's ratio and relative modulus of elasticity vs cell internal angle.
(a): Influence of the cell internal angle on Poisson's ratio for $\alpha=1$, $\beta=0.2$ and $\varphi=45^\circ$.
(b): Influence of the cell internal angle on the relative shear modulus (G_{12}/E_S) for diverse cell configurations and deformation mechanisms ($\alpha=1$, $\beta=0.2$ and $\varphi=45^\circ$).
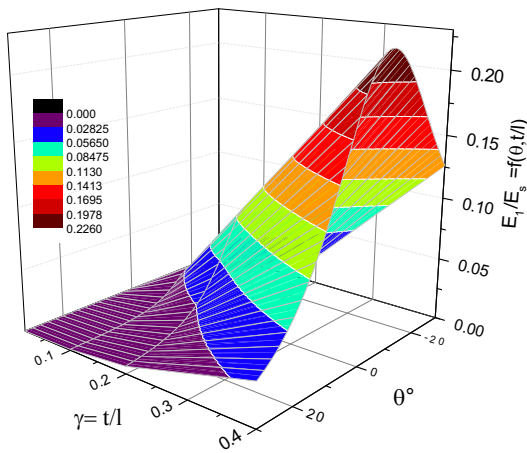
Figure 8-a
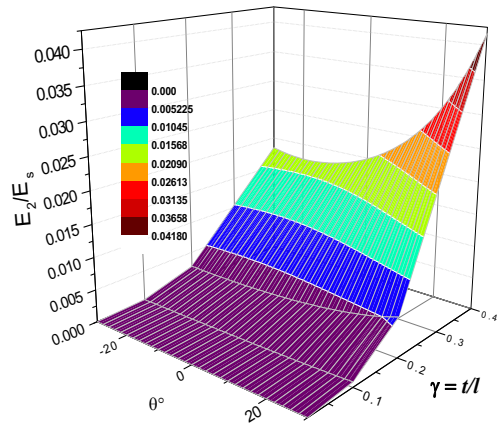
Figure 8-b

Figure 8 – Effect of the wall thickness.
(a): Non-dimensional Young's modulus (E_1/E_S) vs wall thickness ratio ($\gamma=t/l$) for $\alpha=1$, $\beta=0.2$ and $\varphi=45^\circ$.
(b): Non-dimensional Young's modulus (E_1/E_S) vs internal cell angle (θ) and wall thickness ratio ($\gamma=t/l$) for $\alpha=1$, $\beta=0.2$ and $\varphi=45^\circ$.
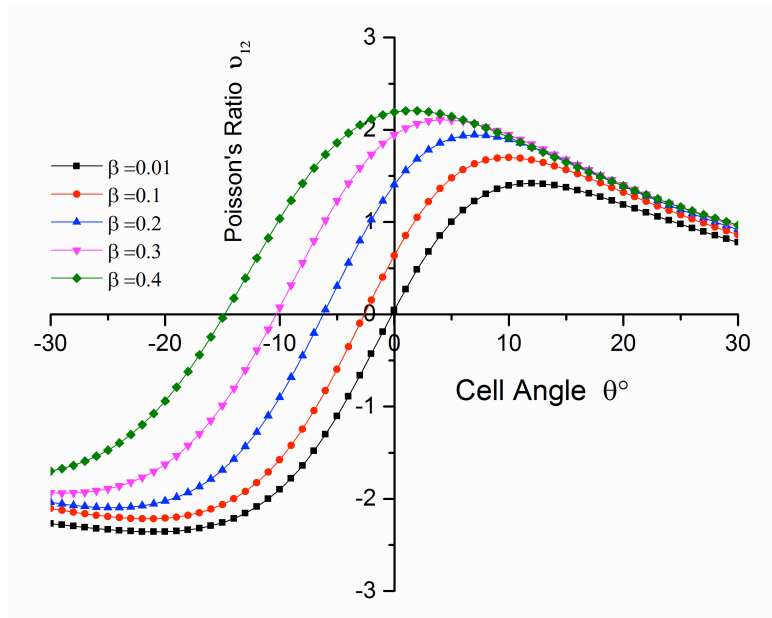
Figure 9 – Poisson's ratio (ν_{12}) vs internal cell angle (θ) and wall base aspect ratio ($\beta=a/l$).
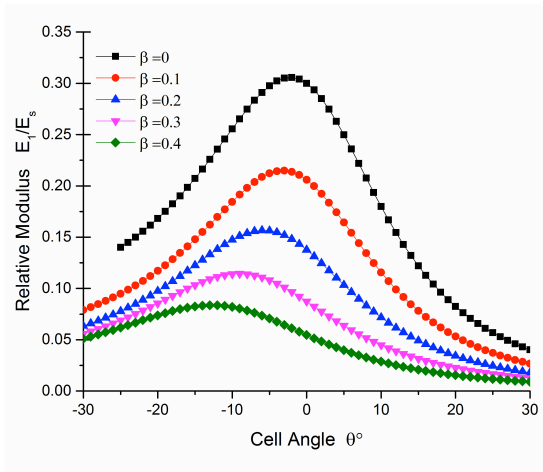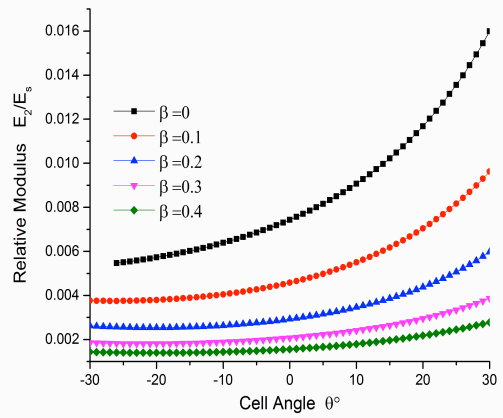

Figure 10-a

Figure 10-b

Figure 10 – Effect of the wall base 'a' ($\beta= a/l$).
(a): Non-dimensional Young's modulus (E_1/E_S) vs wall base aspect ratio ($\beta= a/l$) for $\alpha=1$, $\gamma=0.3$ and $\varphi=45^{\circ}$.
(b): Non-dimensional Young's modulus (E_2/E_S) vs wall base aspect ratio ($\beta= a/l$) for $\alpha=1$, $\gamma=0.3$ and $\varphi=45^{\circ}$.
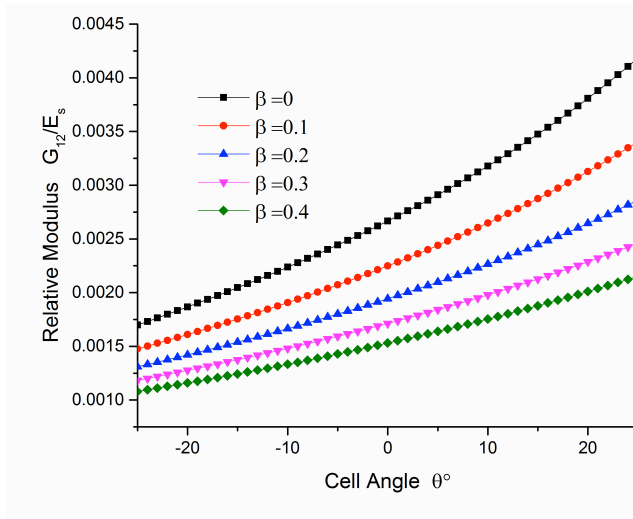
Figure 11 – Effect of the wall base 'a' ($\beta = a/l$). Non-dimensional shear modulus (G_{12}/E_S) vs internal cell angle for different wall base aspect ratios ($\beta = a/l$) for $\alpha=1$, $\gamma=0.2$ and $\varphi=20^{\circ}$.
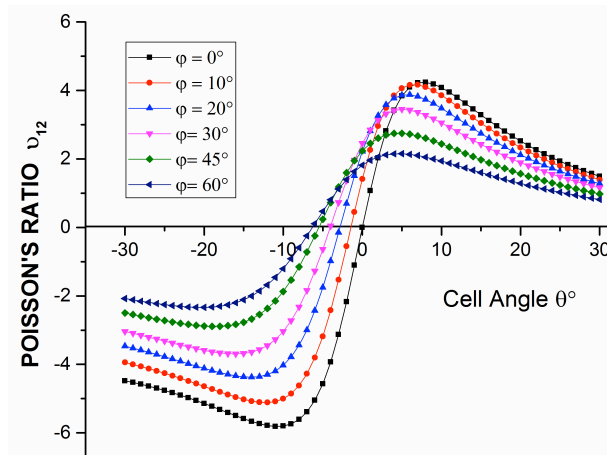

Figure 12 – Cell angle dependence of the in-plane Poisson's ratio.

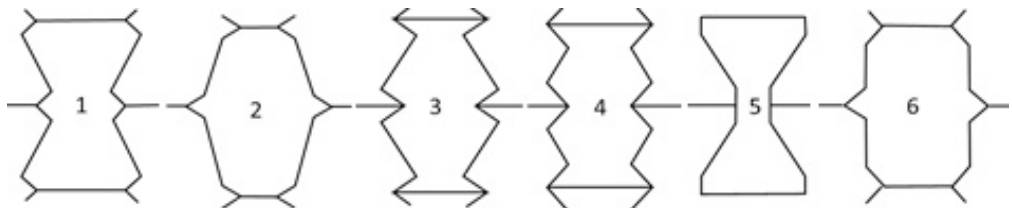| Type	Cell configuration	SHEAR MODULUS G_{12}		POISSON'S RATIO v_{12}		POISSON'S RATIO v_{21}	
		Refined	F.E.A	Refined	F.E.A	Refined	F.E.A
01	α=1.341, β=0.317, γ=0.0178, ϕ= +45.00°, θ= −26.57°	0.05140	0.0534	-2.582	-2.531	-0.303	-0.294
02	α=0.630, β=0.353, γ=0.0063, ϕ= +63.43°, θ= + 21.00°	0.013877	0.0140	1.281	1.2992	0.550	0.5715
03	α=1.370, β=0.430, γ=0.0030, ϕ= −53.10°, θ= + 31.00°	0.009508	0.0097	2.223	2.2555	0.239	0.2467
04	α=1.410, β=0.330, γ=0.1180, ϕ= −45.00°, θ= + 45.00°	18.63196	19.265	0.977	1.0138	0.828	0.8703
05	α=1.600, β=0.200, γ=0.0040, ϕ= 00.00°, θ= − 36.87°	0.000317	0.0003	-1.818	-1.773	-0.487	-0.468
06	α=1.330, β=0.470, γ=0.0060, ϕ= 45.00°, θ= 00.00°	0.002649	0.0027	2.718	2.7601	0.168	0.161

Table 1 – In-plane shear modulus for different cell configurations